

Inhibition of MEG3 ameliorates cardiomyocyte apoptosis and autophagy by regulating the expression of miRNA-129-5p in a mouse model of heart failure

Shan Mi^{a*}, Feng Huang^{a*}, Mingli Jiao^{a,b}, Zhuang Qian^{c*}, Mingming Han^a, Zheng Miao^a and Heqin Zhan^a

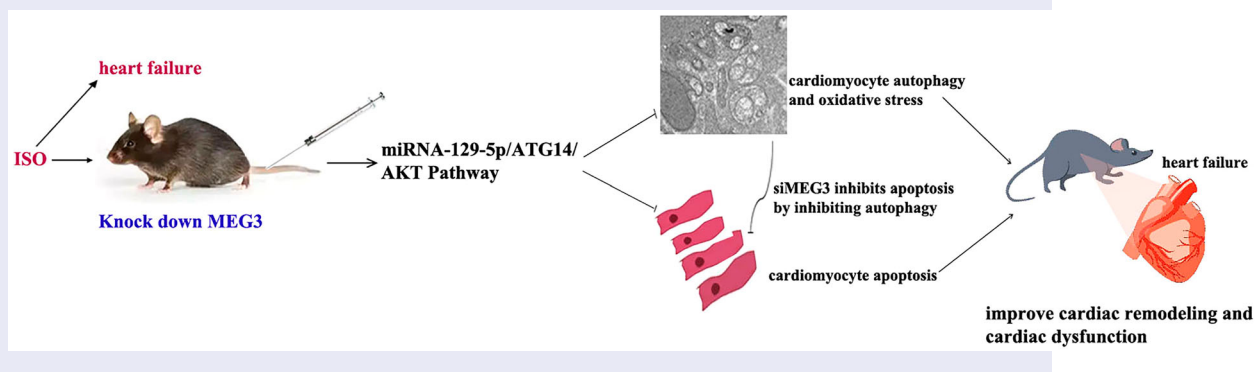
^aDepartment of Pharmacology, College of Pharmacy, Xinxiang Medical University, Xinxiang, Henan, People's Republic of China; ^bExperimental Teaching Center of Public Health and Preventive Medicine, School of Public Health, Xinxiang Medical University, Xinxiang, Henan, People's Republic of China; ^cInstitutes of Health Central Plains, Xinxiang Medical University, Xinxiang, Henan, People's Republic of China.

ABSTRACT

The long non-coding RNA, maternally expressed gene 3 (MEG3), are involved in myocardial fibrosis and compensatory hypertrophy, but its role on cardiomyocyte apoptosis and autophagy in heart failure (HF) remains unclear. The aim of this study was to investigate the effect of MEG3 on cardiomyocyte apoptosis and autophagy and the underlying mechanism. A mouse model of HF was established by subcutaneous injection of isoproterenol (ISO) for 14 days, and an in vitro oxidative stress injury model was replicated with H₂O₂ for 6 h. siRNA-MEG3 was administered in mice and in vitro cardiomyocytes to knock down MEG3 expression. Our results showed that cardiac silencing of MEG3 can significantly ameliorate ISO-induced cardiac dysfunction, hypertrophy, oxidative stress, apoptosis, excessive autophagy and fibrosis induced by ISO. In addition, inhibition of MEG3 attenuated H₂O₂-induced cardiomyocyte oxidative stress, apoptosis and autophagy in vitro. Downregulation of MEG3 significantly inhibited excessive cardiomyocyte apoptosis and autophagy induced by ISO and H₂O₂ through miRNA-129-5p/ATG14/Akt signaling pathways, and reduced H₂O₂-induced cardiomyocyte apoptosis by inhibiting autophagy. In conclusion, inhibition of MEG3 ameliorates the maladaptive cardiac remodeling induced by ISO, probably by targeting the miRNA-129-5p/ATG14/Akt signaling pathway and may provide a tool for pharmaceutical intervention.

KEYWORDS

Heart failure; ISO; oxidative stress; apoptosis; autophagy; MEG3; miRNA-129-5p; ATG14





1. Introduction

Heart failure (HF) is the end stage of various heart diseases, and is a major cause of morbidity and mortality worldwide. The disease has a mortality rate of more than 30% in the first year after diagnosis, and places a significant burden on healthcare systems worldwide due to its progressive nature and frequent hospitalizations [1]. Myocardial infarction, overloaded and valvular disease are common causes of HF. Although much progress has been made in understanding the pathogenesis and treatment of HF, the current situation remains a cause of concern.

The underlying pathology of HF is abnormal cardiac remodeling. In the compensatory phase, the myocardium in a long-term overloaded state becomes hypertrophic under the action of neurohumoral factors and other growth-

promoting substances, and the accompanying apoptosis of cardiomyocytes results in progressive loss of effective contractile units. To compensate for the functional loss, adaptive hypertrophy of the remaining cardiomyocytes develops, as well as extracellular matrix deposition and reactive interstitial fibrosis. The progression of myocardial hypertrophy often leads to myocardial ischemia and hypoxia as well as excessive oxidative stress, and cardiomyocyte autophagy and apoptosis [2], severely compromising cardiac function. This eventually leads to the decompensatory phase of HF. Currently, there is no specific treatment to reverse the pathological cardiac remodeling and reduce the mortality and morbidity of HF. Therefore, the discovery of new cardiac remodeling molecules or regulatory mechanisms is of great importance for the prevention and treatment of HF.

CONTACT Heqin Zhan  xiaofei1@126.com  Department of Pharmacology, College of Pharmacy, Xinxiang Medical University, Xinxiang, Henan 453003, People's Republic of China

*These authors contributed equally to this work.

© 2023 The Author(s). Published by Informa UK Limited, trading as Taylor & Francis Group

This is an Open Access article distributed under the terms of the Creative Commons Attribution-NonCommercial License (<http://creativecommons.org/licenses/by-nc/4.0/>), which permits unrestricted non-commercial use, distribution, and reproduction in any medium, provided the original work is properly cited. The terms on which this article has been published allow the posting of the Accepted Manuscript in a repository by the author(s) or with their consent.

Recently, some studies have found [3,4] that the expression of MEG3 in mouse heart was significantly increased in myocardial fibrosis and compensatory cardiac hypertrophy induced by transverse aortic constriction, and silencing of MEG3 ameliorated these situations. However, the effect and mechanism of MEG3 on cardiomyocyte apoptosis and autophagy in cardiac remodeling in HF are still unclear. Studies have shown that miR-129-5p is a target of MEG3, and knockdown of MEG3 or upregulating of miR-129-5P enhances the protective effect of dexmedetomidine on neonatal mice with hypoxic-ischemic brain injury [5]. Zhang et al. found that miR-129-5P inhibited H₂O₂-induced autophagy and apoptosis of H9C2 cells by regulating the PI3 K/Akt/mTOR signaling pathway through ATG14 [6]. Based on these studies, it can be hypothesized that MEG3 may play an important role in the apoptosis and autophagy of cardiomyocytes by regulating the miR-129-5p/ATG14/Akt signaling pathway. Our previous preliminary experiments found that MEG3 was increased in the left ventricle of ISO-induced mouse HF, but the effect of siRNA-MEG3 on ISO-induced cardiomyocyte apoptosis and autophagy and its mechanism have not been investigated.

ISO is one of the catecholamine adrenergic receptor agonists that has been shown to cause myocardial necrosis, myocardial hypertrophy, fibroblast proliferation, and abnormal systolic-diastolic function by subcutaneous injection, and these ISO-induced cardiac changes can mimic the pathological changes in cardiac tissue during human heart failure [7]. Therefore, this study mainly used the ISO-induced HF mouse model combined with in vitro cell experiments to investigate the effect of MEG3 inhibition on cardiomyocyte apoptosis and autophagy and its mechanism.

2. Materials and methods

2.1. Mice

Adult male C57BL/6 mice, specific-pathogen-free (SPF) grade, 21~25 g, 7~8 weeks old, were obtained from the Beijing Sperford Experimental Animal Center (certificate number: 1103241911015209). All the mice were housed in the animal facilities of Xinxiang Medical University under a controlled ambient temperature 22 ± 2°C with 50%±5% relative humidity and a 12 h light/ 12 h dark cycle (lights on at 7:30 am). Water and food were provided ad libitum. All animal experiments were conducted in accordance with international ethical guidelines and the guidelines of the Ministry of Science and Technology of the People's Republic of China and were approved by the Animal Ethics Committee of Xinxiang Medical College (No: XYLL2016-B001, December 6, 2016 – December 6, 2018).

2.2. Animal grouping, ISO model in vivo and siRNA-MEG3 treatment

Mice were randomly divided into 4 groups: control group, ISO group, ISO + siRNA-NC group and ISO + siRNA-MEG3 group, with 12 mice in each group. Mice were subcutaneously injected with ISO (Solarbio science&technology co., Ltd., Beijing, China) at a dose of 5 mg/kg/day (2.5 mg/kg, twice daily) for 14 days to induce HF according to the previous literature [8]. Left ventricular ejection fraction (LVEF) < 45% by in vivo echocardiography was defined as HF. Mice in the

ISO + siRNA-NC and ISO + siRNA-MEG3 groups were separately injected with siRNA-NC (negative control drug) and siRNA-MEG3 via the tail vein separately with a dose of 2.5 mg/kg once daily for 3 days. Mice in the control and ISO groups were injected with the same volume of saline, respectively.

2.3. Echocardiography and relative centroid mass index

Left ventricular (LV) function in mice was measured by echocardiography on the day after the last dose. Mice were anesthetized with 2~4% (v/v) isoflurane by inhalation. Cardiac dimensions and contractile functions were assessed by noninvasive transthoracic echocardiography using a MS-400 mouse radiofrequency probe in the Vevo 2100 imaging system (Visual Sonics Inc., Toronto, Canada) with a 15 MHz transducer. Evaluation of all cardiac parameters was performed in two-dimensional M-mode images at the level of the papillary muscle and averaged over at least three consecutive cardiac cycles. LVPW (left ventricular posterior wall thickness), IVS (interventricular septum thickness), LVID (left ventricular internal dimension), LVVol (left ventricular volume), left ventricular fractional shortening (LVFS), and LVEF were determined. The mice were then weighed and sacrificed, and the hearts were removed and weighed. The relative centroid mass index was calculated by heart weight/body weight (HW/BW). Then, LV tissue was preserved for further analysis according to the requirements of subsequent experiments.

2.4. Cell culture and intervention

H9C2 rat cardiomyocytes (ATCC, Virginia, USA) were cultured and maintained in the DMEM medium (HyClone, Logan, USA) supplemented with 100 U/mL of penicillin, 100 µg/mL of streptomycin (Beyotime Biotechnology, Shanghai, China), and 10% (v/v) of FBS (Pan-Biotech GmbH, Aidenbach, Germany) at the condition of 37 °C and 5% (v/v) of CO₂. When the cells grew to a density of 80%~90% in the culture medium, cell passage was performed. The medium was changed 2~3 times per week.

H9C2 cells were generally divided into the following six groups: normal control group (control), model group (H₂O₂), negative control group (siRNA-NC), siRNA-NC + H₂O₂ group, siRNA-MEG3 (MEG3 inhibitor) group and siRNA-MEG3 + H₂O₂ group. In addition to the above groups, cells in the ROS level study were also divided into the following six groups for further research: Control group, model group (ISO), siRNA-NC group, ISO + Tiron group, ISO + siRNA-MEG3 group, ISO + Tiron + siRNA-MEG3 group.

Cells were inoculated into different types of culture plates. When the degree of cell fusion reached about 80%, cells in the siRNA-NC group and siRNA-MEG3 group were transferred with siRNA-NC (5'-UUCUCCGAACGUGUCACGUTT-3', 5'-ACGUGACACGUUCGGAGAATT-3') and siRNA-MEG3 (5'-CCUCCUCCACC UCC AAUUUTT-3', 5'-AAAUUGGAGGUGAGGAAGGTT-3') with Lipofectamine 3000 reagent for 24 h, respectively. Cells in other groups were not transfected. After transfection, the cells in the model group were exposed to 100 µM H₂O₂ solution (6 h) or 200 µM ISO solution (24 h) in DMEM without FBS to simulate oxidative damage model in vitro [9,10], and the cells in the Tiron group were administrated 100 µmol/L

Tiron for 2 h [11]. Cells in the other groups were treated with the same amount of DMEM without FBS. Cells from each group were then collected for the subsequent experiments.

2.5. HE/Masson's trichrome/Picrosirius staining

Left ventricular tissue was fixed in 10% (v/v) of formalin buffer for 24 h at 4 °C, dehydrated in gradient alcohol, permeabilized with xylene and embedded in paraffin. Paraffin-embedded tissues were serially sectioned at 5 µm. Sections were stained with hematoxylin and eosin (HE) and Masson's trichrome staining as previously described [12]. One section from each mouse was selected for analysis under a microscope (Olympus, Tokyo, Japan), and the upper and lower fields of each section were observed and photographed. The cross-sectional area (CSA) of cardiomyocytes was measured using Image J analysis software (NIH, MD, USA). Collagen deposition was quantitatively analyzed by collagen volume fraction (CVF) using same imaging software. The calculation formula of CVF in each view of the section is as follows: $CVF = \text{collagen area} / \text{total area} \times 100\%$.

Picrosirius staining was performed according to the method provided in the kit instructions (Beijing Solarbio Science & Technology Co., Ltd., Beijing, China), followed by observation and photography using an EX33 series polarized light microscope (Ningbo sunny instruments Co., Ltd., Zhejiang, China). The percentage of positive collagen fiber areas was statistically analyzed using Image Pro Plus software.

2.6. Detection of autophagy by transmission electron microscopy (TEM)

Autophagy of mouse LV tissue were observed by TEM according to a previously described protocol [13]. Briefly, LV samples were placed in 4% (v/v) glutaraldehyde (Leagene Biotechnology Co., Ltd., Beijing, China) at 4 °C for 6 h and postfixed in 1% (w/v) osmium acid fixative for 2 h. Then, LV tissues in each group were stained with 4% (w/v) uranyl acetate, dehydrated, infiltrated, and embedded in epoxy resin. 60 nm ultrathin sections were cut with an ultrathin slicer (Leica UC6, Wetzlar, Germany), and imaged with a HT7700 transmission electron microscope (Hitachi, Tokyo, Japan).

2.7. Cell apoptosis detection

Cell apoptosis was assessed by flow cytometry using Annexin V-FITC/PI kit (Nanjing KeyGen Biotech. Inc., Nanjing, China) according to the manufacturer's protocol. Briefly, after administration, H9C2 cells were collected with ethylenediaminetetraacetic acid-free trypsin and washed with PBS twice. Then, the cells were resuspended in 200 µL of binding buffer, mixed with 2 µL of annexin V-FITC (fluorescein isothiocyanate) and 2 µL of propidium iodide (PI), and incubated at room temperature for 10 min in the dark. The apoptotic rate of the cells was analyzed using an Attune[®]NxT Acoustic focused flow cytometer (Thermo Fisher Scientific, Massachusetts, USA). The percentage of apoptotic cells was calculated after treatment using computer software. Apoptotic rate = number of apoptotic cells / (number of apoptotic cells + normal cells) × 100%.

2.8. ROS level/GFP-LC3B detection

Reactive oxygen species (ROS) production was detected by an ROS-sensitive fluorescent indicator using dihydroethidium (DHE) assay kit (Beyotime Biotechnology, Shanghai, China). Briefly, the H9C2 cells were seeded in 24-well plates (5×10^4 cells/well) with 2 µM DHE solution at 37 °C for 30 min, and then the cells were washed for 3 times with PBS. ROS generation was represented by the total DHE fluorescence, and fluorescence intensity was observed and imaged with the inverted fluorescence phase contrast microscope (Nikon Corporation, Tokyo, Japan). The fluorescence intensity was analyzed using Image J software (NIH, Bethesda, MD).

GFP-LC3 plasmid was used to infect H9C2 cells for autophagy detection.

In brief, the H9C2 cells were inoculated into a 24-well plate (5×10^4 cells/well), then plasmid containing GFP-LC3B was transfected into the cells with lipofectamine 3000 for 48 h according to the manufacturer's protocol. Images of cells were captured under a fluorescence phase contrast microscope (Nikon Corporation, Tokyo, Japan).

2.9. RT-qPCR (Quantitative real-Time) assay

Gene expression levels were quantified by real-time PCR. Total RNA was extracted from mouse LV tissue and H9C2 cells using Trizol reagent (Life Technologies, Carlsbad, USA). The total concentration of RNA was measured using an ultra-micro spectrophotometer (Implen GmbH, Munich, Germany), and the purity and degeneration of RNA were detected by OD260/OD280 and agarose gel electrophoresis, respectively. When OD260/OD280 was between 1.8 and 2.1, agarose gel electrophoresis showed three bands of 5S, 18S, and 28S without dispersion (5S band is darker). The brightness of the 28S band was twice that of the 18S band, indicating the high purity and non-degraded RNA, the follow-up experiments were then carried out. In the mRNA experiment, 1 µg RNA was reverse transcribed into cDNA using HiScriptRQ RT SuperMix for qPCR (+gDNA wiper) kit (Vazyme Biotech Co., Ltd, Nanjing, China). For the miRNA experiment, 5 µg RNA was reverse transcribed into cDNA using the All-in-One TMmiRNA First-Strand cDNA Synthesis Kit (GeneCopoeia, MD, USA). The expression level of the gene was then analyzed by qPCR. β-actin was used as an internal reference control. The qPCR cycling conditions were as follows: 95 °C for 5 min; 40 amplification cycles at 95 °C for 10 s, 60 °C for 30 s and 95 °C for 15 s. The sequences of the primers were as follows: miRNA-129-5p (5'-ACATCTTTTTGCGTCTGGGCTTGC-3'; 5'-TGGTGTCTGGAGTCG-3'), LncRNA-MEG3 (5'-GTGAAGGTCGGAGTCGAACG-3'; 5'-CTCGCTCTGGAAGATGGTG-3'), U6 (5'-CTCGCTTCGGCAGCACA-3'; 5'-AACGCTTCACGAATTTGCGT-3') and β-actin (5'-AGGGAAATCGTGCCTGACAT-3'; 5'-AACCGCTCATTGCCGATG-3'). The PCR product was verified by melting curve analysis, and the relative expression level of the target gene was analyzed using the $2^{-\Delta\Delta Ct}$ method.

2.10. Western blotting

Total protein in the LV tissue and H9C2 cells was extracted with RIPA buffer (Beyotime Biotechnology, Shanghai, China), and the protein concentration was measured using the BCA protein assay kit (Beyotime Biotechnology, Shanghai, China). The protein was separated by sodium dodecyl sulfate-

polyacrylamide gel electrophoresis (SDS-PAGE), and was transferred to a polyvinylidene fluoride (PVDF) membrane. The membrane was then incubated in 5% (w/v) nonfat dry milk for 2 h at room temperature, followed by incubation with primary antibodies (Affinity Biosciences LTD., OH, USA) incubation at 4 °C overnight. The primary antibodies include anti-p-Akt, Akt, Beclin1 (1:800); anti-p-GSK3 β , GSK3 β (1:700); anti-p-mTOR, mTOR (1:700); anti-Bcl2, Bax, p62 and ATG14 (1:800); anti-NPPA, NPPB, MYH7 and LC3A/B (1:500). The secondary antibody was then added at 1:5000 and incubated for 2 h at room temperature. Then, the blots were developed with ECL reagent (Affinity Biosciences LTD., OH, USA) and visualized with iBright 1500 gel imaging system (Invitrogen, CA, USA). The gray value of the band was determined using Image J analysis software (NIH, MD, USA). The amount of signal was normalized to GAPDH.

2.11. Statistical analysis

Data are presented as the mean \pm SD. All calculations were performed using SPSS program version 19.0 and Graphpad Prism v5.0. The Shapiro-wilk method was used to determine the normal distribution of all data. For data with normal distribution, comparisons between experimental groups were made by One-way ANOVA followed by LSD or Dunnett-T3 method; for non-normally distributed data, comparisons between experimental groups were made by using nonparametric independent samples test followed by Kruskal-Wallis method. $P < 0.05$ was considered to be statistically significant.

3. Restuls

3.1. siRNA-MEG3 ameliorates murine cardiac function and tissue structure in HF

Cardiovascular-related diseases such as myocardial infarction, pressure overload, and volume overload can lead to myocardial cell injury, maladaptive cardiac remodeling and functional abnormalities, and eventually heart failure due to low left ventricular pumping or filling. Our preliminary experiments showed that the expression of the MEG3 gene was significantly increased in the heart of ISO-induced HF mice and in H₂O₂-stimulated H9C2 cells compared with the Control group. This suggests that MEG3 may mediate maladaptive cardiac remodeling in ISO-induced HF. Therefore, we first investigated the effects of siRNA-MEG3 on cardiac function and left ventricular changes in a mouse model of HF induced by ISO. As shown in Figure 1(a), ISO induced the following changes compared with the Control group: a decrease in LVEF, LVFS, LVPW, and IVS; an increase in heart weight/body weight ratio, LVID and LVVol ($P < 0.01$); while the treatment with siRNA-MEG3 reversed the above results, the negative control group (ISO + siRNA-NC) did not show significant changes in the above parameters compared with the ISO group ($P > 0.05$).

We then investigated the effect of siRNA-MEG3 on the pathological changes of the LV of ISO-induced HF mice. Figure 1(b) HE staining results showed that cardiomyocytes in the control group showed an orderly arrangement with normal cell morphology, whereas in the ISO group marked hypertrophy and a small amount of cell necrosis, nuclear lysis and inflammatory cell infiltration were observed (as indicated by the green arrow), and the cardiomyocyte cross-sectional area (CSA) was significantly increased compared

with the control group. Inhibition of MEG3 significantly improved the pathological morphology of cardiomyocytes and reduced the increase in CSA induced by ISO.

Because myocardial fibrosis can restrict the movement of cardiomyocytes and cause an increase in myocardial stiffness and a decrease in ventricular wall compliance, thereby affecting the systolic and diastolic function of the heart, the degree of left ventricular fibrosis of mice in each group was also evaluated by Masson's trichrome staining and picosirius red staining, respectively. Masson's trichrome staining revealed (Figure 1(c)) that large areas of myocardial fibrosis were often observed in the ISO group (as shown by the black arrow shows), and the CVF value was significantly higher than that of the control group ($P < 0.01$); inhibition of MEG3 significantly blunted the increase in myocardial fibrosis area and CVF values induced by ISO ($P < 0.01$). Furthermore, we identified deposited collagen I (strong orange or bright red, indicated by green arrow) and collagen III (green staining, indicated by white arrow) by picosirius staining. The results in Figure 1(d) showed that ISO induced increased deposition of collagen I and collagen III (more collagen I deposited than collagen III), while inhibition of MEG3 could simultaneously reduce the deposition of these two collagens in the left ventricular tissue of mice in the ISO group. Moreover, siRNA-NC had no significant effect on the cardiomyocyte damage, hypertrophy and fibrosis induced by ISO. These results suggest that siRNA-MEG3 can ameliorate ISO-induced reduction of cardiac function, cardiomyocyte damage, hypertrophy and severe fibrosis in mice.

3.2. siRNA-MEG3 reduces the protein expression levels of HF marker in murine LV and H₂O₂-stimulated H9C2 cells

To further observe the effect of siRNA-MEG3 on various cardiac remodeling markers, we detected the expression levels of NPPA (natriuretic peptide A), NPPB (natriuretic peptide B) and MYH7(β -myosin heavy chain) proteins by Western blotting. Figure 2(a) showed that the ratios of NPPA/GAPDH, NPPB/GAPDH and MYH7/GAPDH were significantly increased in the ISO group compared with the control group ($P < 0.01$), whereas siRNA-MEG3 treatment markedly decreased their expressions in the LV compared with the ISO group ($P < 0.01$). The progression of HF is not only closely related to the continuously increased levels of cardiac hormones, but also involves excessive oxidative stress response. Therefore, we determined the effect of siRNA-MEG3 treatment on NPPA, NPPB and MYH7 protein expression of H₂O₂-stimulated H9C2 cells in vitro. In Figure 2(b), Western blot analysis revealed that the expression levels of NPPA, NPPB and MYH7 protein were significantly increased in the H₂O₂ model group ($P < 0.01$), while the above effects induced by H₂O₂ were reversed by siRNA-MEG3 treatment ($P < 0.01$). These results indicate that siRNA-MEG3 can effectively inhibit the markers of ISO-induced HF and H₂O₂-induced oxidative damage in H9C2 cells.

3.3. siRNA-MEG3 reduces the cardiomyocytes apoptosis and ROS level

Under the oxidative stress of HF, continuous apoptosis of cardiomyocytes causes progressive loss of cardiac functional units and severely depresses the contractile function of the heart [2]. Here, we investigated the effect of siRNA-MEG3

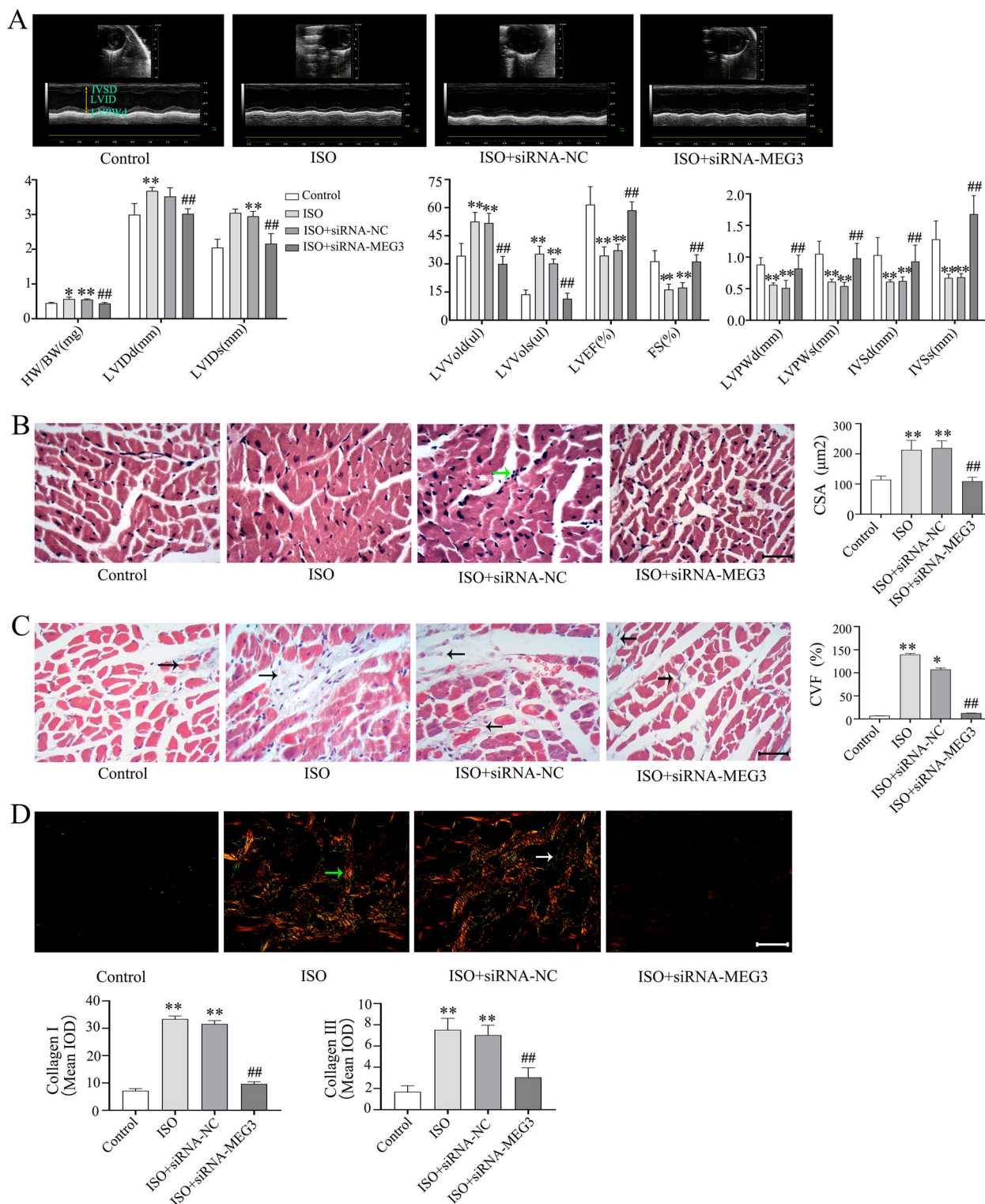


Figure 1. siRNA-MEG3 ameliorates the cardiac function and tissue structure of the LV in ISO-induced murine HF. (A) Representative M mode images of echocardiography in the mice and quantitative analysis of each cardiac function index. (B) Representative HE staining images of LV (scale bar: 100 μ m; cell necrosis, nuclear lysis and inflammatory cell infiltration indicated by green arrows) and quantitative analysis of cross-sectional area (CSA) in the mice. Chromatin in the nucleus and the nucleic acid in the cytoplasm were stained purple-blue, and the components in the cytoplasm and extracellular matrix were stained red. (C) Representative Masson staining images (scale bar: 100 μ m; myocardial fibrosis indicated by black arrows) and quantitative analysis of collagen volume of LV in the mice. Cardiomyocytes were stained red and collagenous fibers stained blue. (D) Representative images of picrosirius staining in mice (scale bar: 100 μ m) and quantitative analysis of collagen I and III of LV in the mice. Collagen I was stained red strong orange or bright red, indicated by green arrow; collagen III was stained green, indicated by white arrow. HW/BW: heart weight/body weight; LVID: left ventricular internal dimension; LVVold: left ventricular volume; LVPW: left ventricular posterior wall; IVS: intraventricular septum; LVEF: left ventricular ejection fraction; FS: fractional shortening; d: diastole; s: systole; LV: left ventricular; CVF: collagen volume fraction. Data are expressed as mean \pm SD. Mice, $n = 12$ (Figure.1 A), $n = 4$ (Figure.1 B-D). ** $p < 0.01$ versus control group; # $p < 0.01$ versus ISO group.

on the expression of apoptosis molecular markers Bcl2 (B-cell lymphoma 2) and Bax (Bcl2-associated X protein) protein in vivo and in vitro by Western blot. Figure 3(a) shows that the expression level of Bcl2/Bax protein was decreased in murine LV of HF induced by ISO compared with the control group ($P < 0.05$), while siRNA-MEG3 treatment reversed the

decrease of Bcl2/Bax protein expression. The experimental results in H9C2 cells in vitro were the same as those conducted in mice (Figure 3(b)). Furthermore, the apoptosis rate and ROS levels of H9C2 cells in vitro were detected by flow cytometry and DHE staining, respectively. As shown in Figure 3(c), the apoptosis rate of H_2O_2 -stimulated H9C2

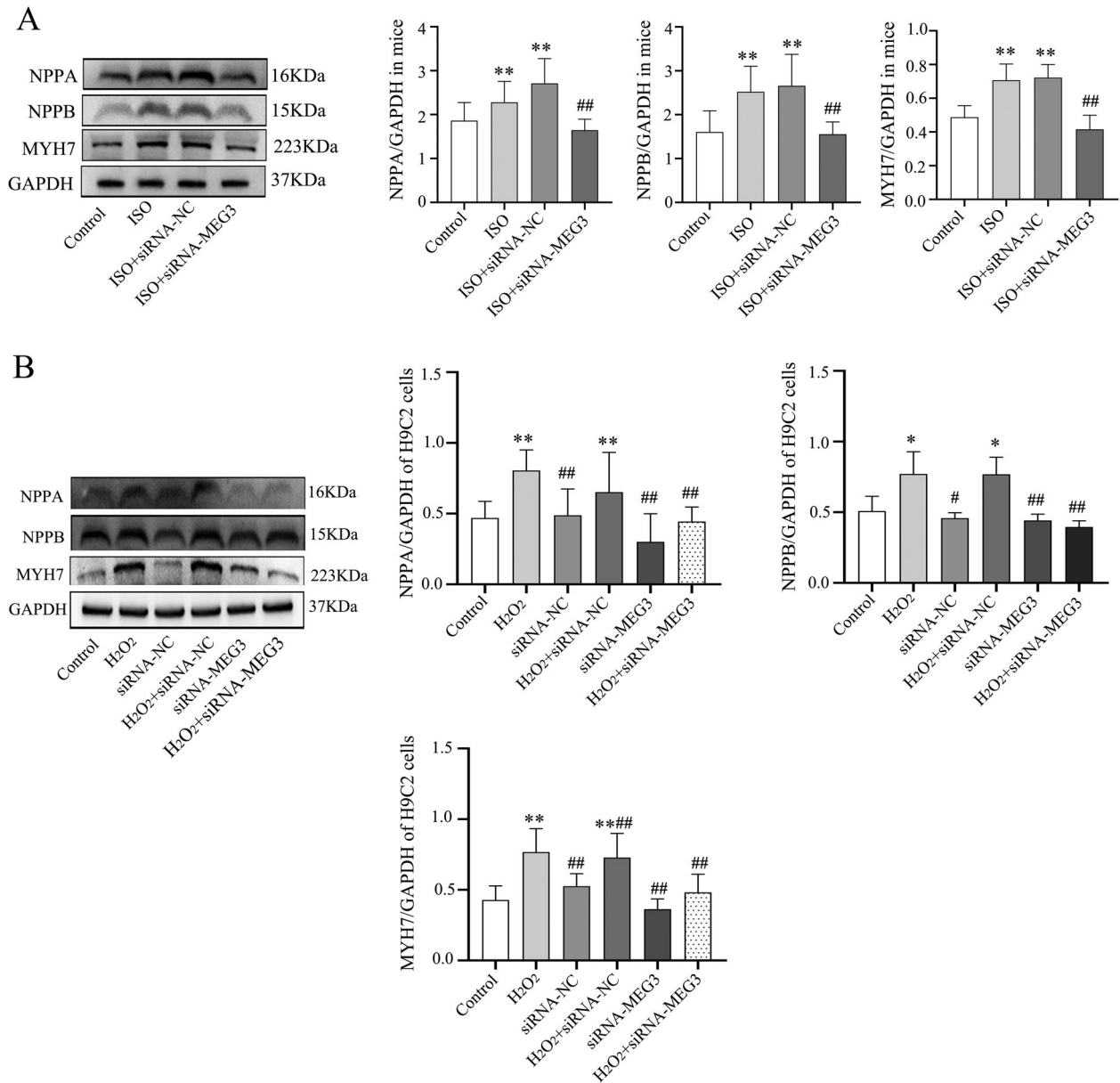


Figure 2. siRNA-MEG3 reduced the expression of cardiac remodeling markers in the LV of mice with HF induced by ISO or oxidative damage of H9C2 cells induced by H₂O₂. (A) Representative western blotting bands of NPPA, NPPB and MYH7 and their quantitative analysis by densitometry based on immunoblot images in the LV of mice. (B) Representative Western blotting bands of NPPA, NPPB and MYH7 and their quantitative analysis in the H9C2 cells. Data are expressed as mean \pm SD. Mice, n = 5; H9C2 cells = 2 batches of cells, repeat 2~3 multiple wells for each batch of cells. * p < 0.05, ** p < 0.01 versus control group; # p < 0.05, ## p < 0.01 versus control group.

cells was greatly increased, whereas siRNA-MEG3 significantly decreased the apoptosis rate ($P < 0.01$). In addition, the DHE staining results of the Figure 3(d) showed that siRNA-MEG3 blunted increase of ROS levels induced by H₂O₂ in H9C2 cells ($P < 0.01$). Figure 3(e) showed that the superoxide anion-specific inhibitor Tiron attenuated the ISO-induced increase in ROS levels, while siRNA-MEG3 had a similar effect. The results suggest that siRNA-MEG3 reduces the cardiomyocytes apoptosis in murine HF, which may be related to its inhibition of ROS activation induced by H₂O₂ or ISO.

3.4. siRNA-MEG3 decreases excessive autophagy in murine LV of HF induced by ISO and H₂O₂-stimulated H9C2 cells

The majority of evidence indicates that dysfunctional myocardial autophagy is an important factor leading to cardiac remodeling and heart failure [14,15], and cardiomyocyte autophagy and

apoptosis have an interaction. Therefore, we investigated the effect of siRNA-MEG3 on cardiomyocyte autophagy induced by ISO and H₂O₂. The results of ultramicroscopic TEM showed that there were a large number of double-membrane autophagosomes in murine left ventricular myocardium of HF caused by ISO, which contained many damaged organelles (Figure 4(a)). Treatment with siRNA-MEG3 significantly reduced ISO-induced autophagy in cardiomyocytes (Figure 4(a)).

GFP-LC3B is one of the markers used to detecting autophagy. In non-autophagy, GFP-LC3B often exists in the cytoplasm in the form of dispersion. When autophagy occurs, GFP-LC3B aggregates on the autophagy membrane. We detected autophagy by transfecting GFP-LC3B plasmid into H9C2 cells. The fluorescence amount of extracellular free GFP-LC3B in the H9C2 cells of oxidative damage induced by H₂O₂ was significantly higher than that in the control group, and autophagosomes were found to be formed between cells, and intracellular vacuoles (Figure 4(b)). After

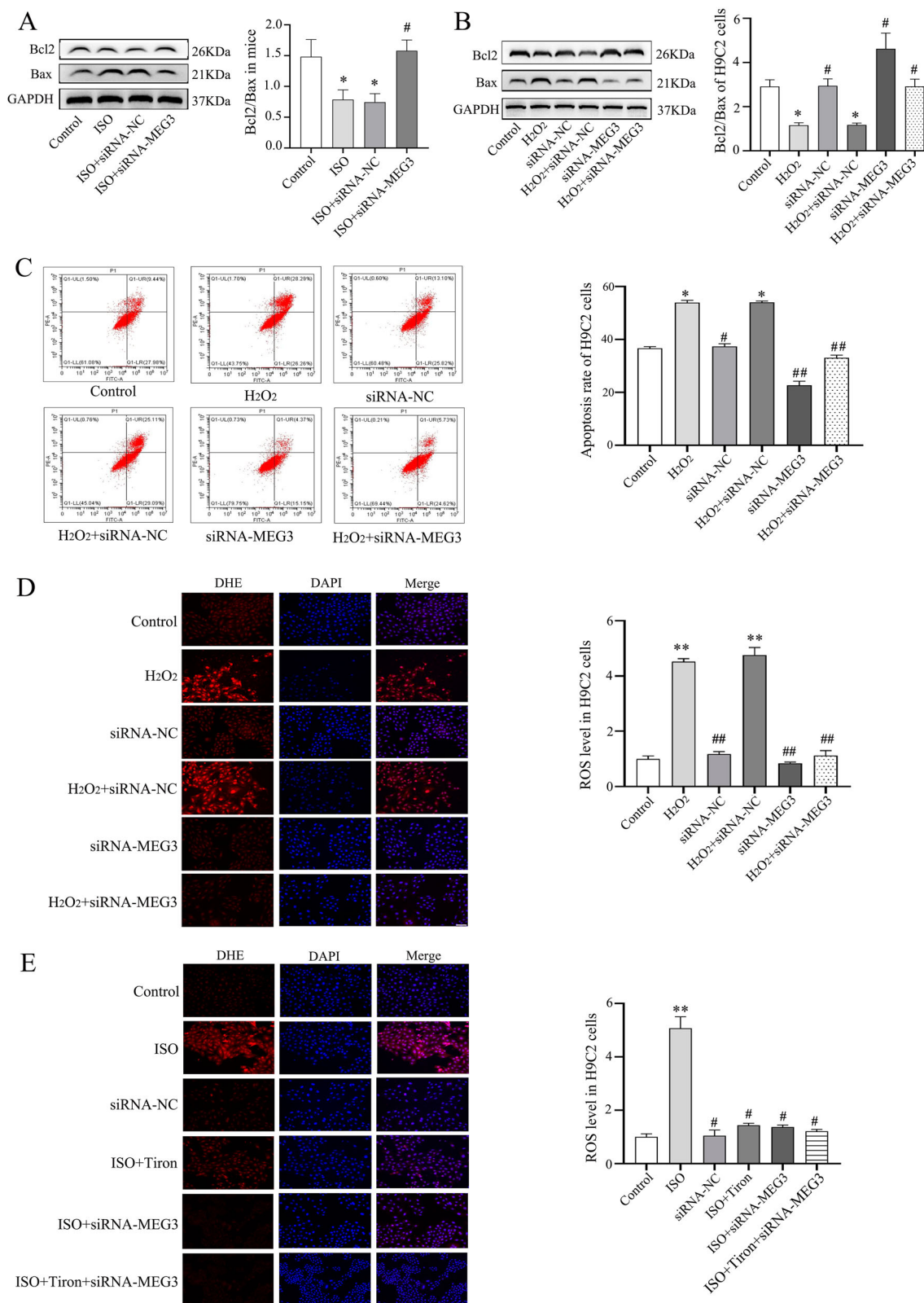


Figure 3. siRNA-MEG3 reduced myocardial apoptosis and ROS level of H_2O_2 -stimulated H9C2 cells. (A-B) Representative western blotting bands of Bcl2 and Bax and their quantitative analysis in the mice and H9C2 cells. (C) Representative images of flow cytometry in H9C2 cells and quantitative analysis of apoptotic cells. (D-E) Representative images of DHE fluorescence staining and quantitative analysis of ROS level in H9C2 cells. The blue fluorescence represents the nucleus stained with DAPI, and the red fluorescence represents ROS (scale bar = 50 μm). Data are expressed as mean \pm SD. Mice, $n = 5$; H9C2 cells = 2 batches of cells, repeat 2~3 multiple wells for each batch of cells. ** $p < 0.01$ versus control group; # $p < 0.05$, ## $p < 0.01$ versus control group.

treatment with siRNA-MEG3, the ultramicroscopic findings were improved. These results indicate that siRNA-MEG3 can significantly reduce the level of autophagy in murine HF, which may improve cardiac remodeling and cardiac function.

In addition, the expression levels of molecular markers of autophagy including Beclin1, LC3 II/LC3 I and p62 protein

were detected by Western blot. Figure 4(c) shows that the expression of Beclin1 and LC3II/LC3I was increased in the LV of ISO-induced HF mice compared with the control ($P < 0.01$ and $P < 0.05$, respectively). Conversely, the expression of p62 protein was decreased in murine LV compared with the control ($P < 0.01$). Treatment with siRNA-MEG3 reversed the

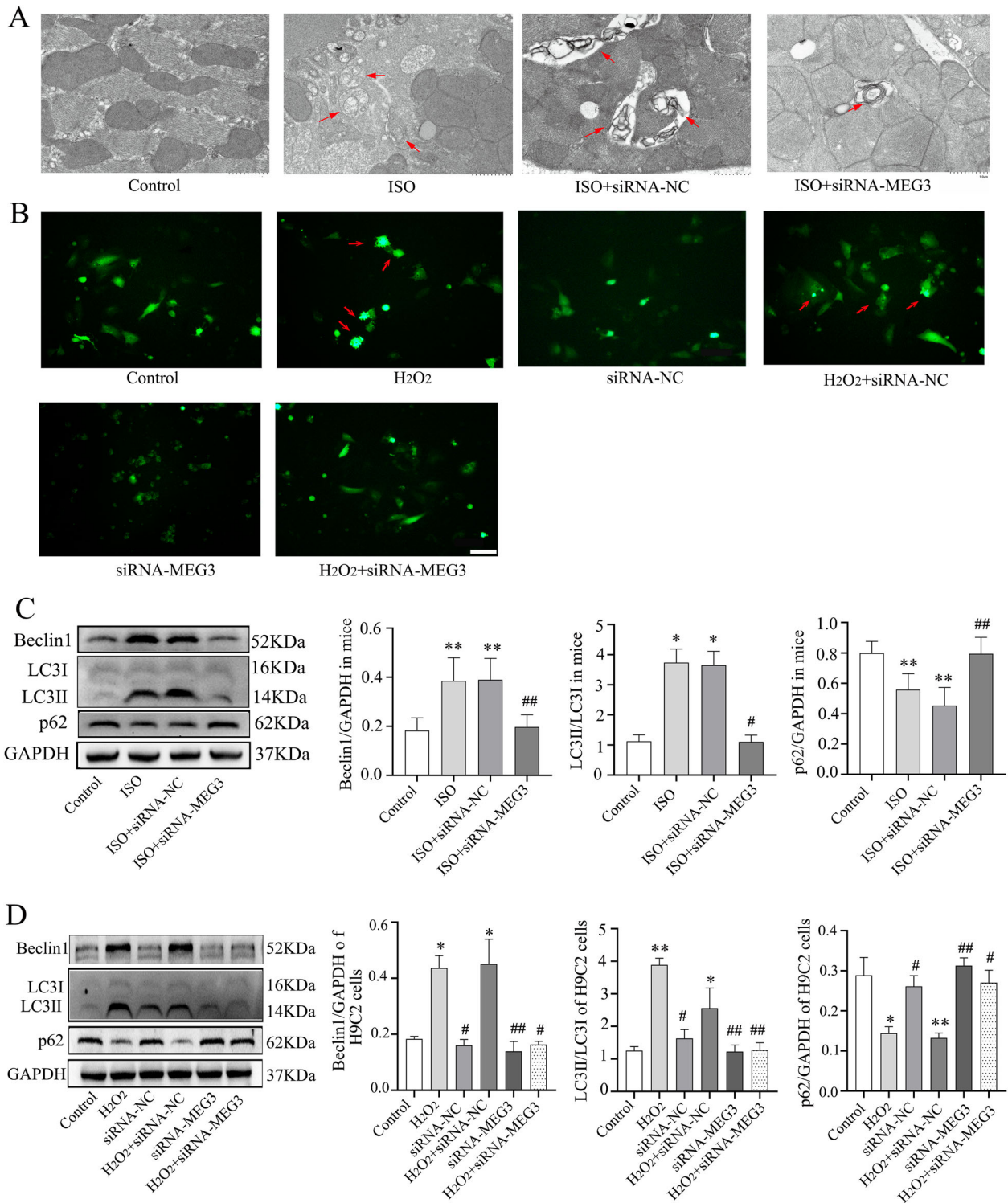


Figure 4. siRNA-MEG3 inhibits autophagy in murine HF induced by ISO in vivo and H₂O₂-stimulated H9C2 cells in vitro. (A) Representative images of left ventricular autophagy in mice were obtained by TEM (scale bars: 1 μ m). The typical tissue autophagosome is indicated by the red arrow. The higher the number of autophagosomes, the higher the autophagy. (B) Fluorescence representative image of H9C2 cells transfected with GFP-LC3B (scale bar: 50 μ m). The red arrow represents free GFP-LC3B and autophagy vacuoles. The more the number, the stronger the autophagy. (C) Western blotting representation image of Beclin1, LC3II/LC3I and p62 proteins in mouse LV and quantitative analysis of Western blotting data. (D) Western blotting representation image of Beclin1, LC3II/LC3I and p62 proteins in H9C2 cells and quantitative analysis of Western blotting data. Data are expressed as mean \pm SD. Mice, n = 5; H9C2 cells = 2 batches of cells, 2–3 multiple wells repeated for each batch of cells. * p < 0.05, ** p < 0.01 versus control group; # p < 0.05, ## p < 0.01 versus control group.

expression of the above proteins in the LV of ISO-induced HF mice. The expression levels of Beclin1, LC3II/LC3I and p62 protein in H9C2 cells are consistent with those the animals (Figure 4(d)). P62 protein is a receptor for selective autophagy and is degraded during autophagy, indicating that the autophagic flux [16]. These results indicated that siRNA-MEG3 could inhibit cardiomyocyte autophagy and affect autophagic flux, thereby improving cardiac function in HF.

3.5. siRNA-MEG3 regulates miRNA-129-5p and its downstream apoptosis signal pathway in vivo and in vitro

To determine whether siRNA-MEG3 regulates the expression of its downstream apoptosis signaling pathway proteins by increasing the transcription level of miR-129-5P, qPCR was used to detect the expression levels of MEG3 and miR-129-

5P genes in murine LV and H9C2 cells, respectively. Furthermore, Western blotting was used to detect the protein expression levels of p-Akt and p-GSK3 β in murine LV and H9C2 cells. The results in Figure 5(a) showed that the expression of MEG3 in the murine LV of the HF model group was significantly higher than that of the control group ($P < 0.01$), whereas the expression of miRNA-129-5p was significantly lower ($P < 0.05$). However, the expression levels of MEG3 and miRNA-129-5p were reversed by siRNA-MEG3 treatment ($P < 0.01$ and $P < 0.05$, respectively). These results indicated that MEG3 negatively interacted with miR-129-5P. The gene expression trend of MEG3 and miRNA-129-5p in H9C2 cells in vitro was consistent with the results of animal experiments (Figure 5(b)).

After determining the regulatory relationship between MEG3 and miRNA-129-5p, we further investigated the effect of the siRNA-MEG3/miRNA-129-5p signaling pathway on the expression of downstream apoptotic proteins. As shown in the Figure 5(c,d), the expression levels of p-Akt and p-GSK3 β protein were significantly decreased in mouse LV of HF and H₂O₂-stimulated H9C2 cells compared with the control ($P < 0.05$ or $p < 0.01$). Treatment with siRNA-MEG3 reversed the decrease in p-Akt and p-GSK3 β protein expression in murine LV of HF induced by ISO and H₂O₂-stimulated H9C2 cells.

3.6. siRNA-MEG3 regulates autophagy-related ATG14/mTOR signaling axis in vivo and in vitro

The treatment of si-MEG3 can ameliorate the excessive autophagy of cardiomyocytes and upregulate the gene expression level of miRNA-129-5p. However, whether it regulates the expression of downstream autophagy-related proteins through miRNA-129-5p gene needs further confirmation. Here, Western blot was used to detect the expression levels of autophagy promoting protein mammalian autophagy-related gene 14 (ATG14) and autophagy inhibitory protein p-mTORC1. Figure 6(a) showed that the expression of ATG14 was increased in the LV of ISO-induced HF mice compared with the control group ($P < 0.05$), and the expression level of p-mTORC1 protein was decreased ($P < 0.01$). siRNA-MEG3 treatment reversed the above results. The results of in vitro cell experiments (Figure 6(b)) are consistent with animal study. These results indicate that si-MEG3 can regulate the ATG14/Akt/mTOR signaling axis by upregulating miRNA-129-5p gene, thereby inhibiting excessive autophagy of cardiomyocytes.

3.7. siRNA-MEG3 reduces H₂O₂-induced cardiomyocyte apoptosis by inhibiting autophagy

To determine the effect of autophagy inhibition by siRNA-MEG3 on oxidative stress-induced apoptosis of cardiomyocytes, the special autophagy inhibitors and agonists were used to interfere with H₂O₂-stimulated H9C2 cells, then the rate of apoptosis and ROS level of cells were detected by the flow cytometry and DHE staining, respectively.

Figure 7 showed that the apoptosis rate and ROS level of H9C2 cells in the H₂O₂ group were significantly higher than those in the control group ($P < 0.05$). 3-Methyladenine (MA), an autophagy inhibitor, decreased the apoptosis and ROS accumulation of H9C2 cells induced by H₂O₂ ($P < 0.01$ and $P < 0.05$, respectively), siRNA-MEG3, which has the same

function as 3-MA also attenuated the apoptosis and increased the ROS level of H₂O₂-stimulated H9C2 cells. However, rapamycin (Rapa), an autophagy inducer, counteracted the above effects of siRNA-MEG3. These results suggest that siRNA-MEG3 may reduce oxidative stress-induced apoptosis by inhibiting autophagy.

4. Discussion

This study was designed to determine whether inhibition of MEG3 could reduce cardiomyocyte apoptosis and autophagy in murine HF and in cultured cells under oxidative stress by regulating miR-129-5P. To achieve this goal, we used subcutaneous injection of ISO to establish a mouse model of HF and a cell model of oxidative damage by H₂O₂. Then, the mouse model of HF and cardiomyocytes with oxidative damage in vitro were treated with siRNA-MEG3, and the corresponding changes were studied.

Our results demonstrated the following novel findings that (1) MEG3 may mediate ISO-induced cardiac dysfunction and excessive cardiac remodeling, while inhibition of MEG3 can ameliorate cardiac dysfunction, abnormal apoptosis, excessive oxidative stress as well as autophagy of cardiomyocytes in murine HF induced by ISO; (2) the mechanism by which MEG3 inhibition reduces cardiomyocyte apoptosis and autophagy may be related to the regulation of miR-129-5P/ATG14/Akt signaling pathway; (3) MEG3 inhibition attenuated cardiomyocyte apoptosis induced by ISO in vivo and H₂O₂ in vitro by attenuating excessive autophagy and oxidative stress.

The pathogenesis of cardiovascular disease involves many complex issues, and increased oxidative stress has been considered as one of the common pathways [17]. Previous studies have shown that an excessive increase of ROS in the heart can lead to maladaptive myocardial remodeling and the progression of heart failure [18,19]. The animal model of ISO-induced myocardial injury has been widely used to study the beneficial effects of drugs on cardiac dysfunction [20]. Continuous β -adrenergic stimulation after ISO administration results in the generation of ROS, cardiomyocyte damage, ventricular hypertrophy and increased fibrosis [21]. In heart failure, mitochondria, the major source of cellular ATP, are key producers of ROS. ROS are a class of single-electron reduction products of oxygen in vivo, and they are generated when electrons, before failing to pass to the terminal oxidase, leak out of the respiratory chain and consume about 2% of oxygen. They mainly include single-electron reduction product of oxygen superoxide anion ($\cdot\text{O}_2^-$), the two-electron reduction product hydrogen peroxide (H₂O₂), the 3-electron reduction products hydroxyl radicals ($\cdot\text{OH}$), as well as nitric oxide derived ROS, such as pernitrate (OONO \cdot^-). Among them, $\cdot\text{O}_2^-$ is an important free radical that can lead to the formation of other ROS such as H₂O₂, $\cdot\text{OH}$ and OONO \cdot^- (which is generated from nitric oxide and superoxide anions). H₂O₂ is an important ROS that is highly permeable to the cell membrane and forms highly reactive $\cdot\text{OH}$ radicals with intracellular ions through the FENTON reaction [22]. Hydroxyl radicals are the major oxidants of cellular damage [23]. In this study, the ISO-induced cardiomyocyte acute injury murine heart failure model and H₂O₂-stimulated cardiomyocytes in vitro were used to evaluate the effect and molecular mechanism of MEG3 inhibition on cardiomyocyte apoptosis and autophagy.

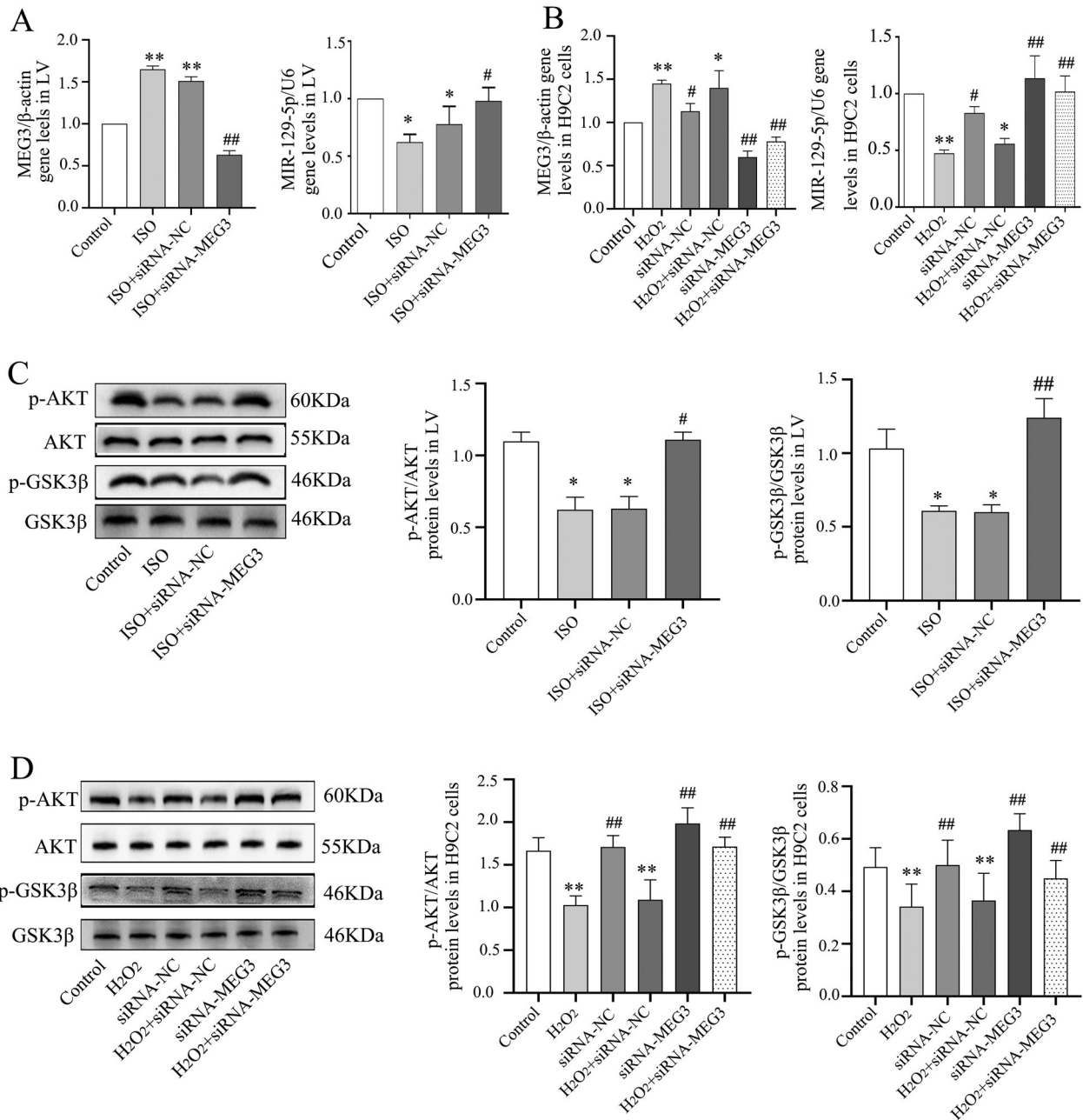


Figure 5. siRNA-MEG3 regulates the expression of miRNA-129-5p and its downstream apoptotic proteins. (A-B) The levels of MEG3 and miRNA-129-5p gene were detected by RT-PCR in LV of mice and H9C2 cells. (C) Representative image of Western blotting of p-Akt, Akt, p-GSK3 β and GSK3 β in mice and their quantitative analysis. (D) Representative image of Western blotting of p-Akt, Akt, p-GSK3 β and GSK3 β in H9C2 cells and their quantitative analysis. Data are expressed as mean \pm SD. Mice, $n = 5$; H9C2 cells = 2 batches of cells, repeat 2~3 multiple wells for each batch of cells. * $p < 0.05$, ** $p < 0.01$ versus control group; # $p < 0.05$, ## $p < 0.01$ versus control group.

We performed cardiac MEG3 knockdown by injecting siRNA-MEG3 to evaluate the effect of MEG3 on mouse cardiac function in response to HF induced by ISO. Our study revealed that siRNA-MEG3 treatment significantly improved cardiac function and remodeling in mice by reducing ISO-induced cardiomyocyte hypertrophy, fibrosis, oxidative stress, apoptosis and autophagy. Pathological hypertrophy and heart failure are evidenced by the over-expression of NPPA, NPPB and MYH7 [24]. Our study showed that ISO induced higher levels of NPPA, NPPB and MYH7 proteins, whereas treatment with siRNA-MEG3 reduced their expressions. The development and progression of HW/BW ratio under different pressures was attributed to the cardiac hypertrophy and accumulation of fibrosis [25]. Our results confirmed that ISO caused a significant increase in the HW/BW ratio, whereas

inhibition of MEG3 reversed the HW/BW ratio and reduced the collagen volume fraction.

After analyzing the effect of siRNA-MEG3 on ISO-induced myocardial fibrosis in mice using Masson's trichrome staining, we further examined myocardial fibrosis in each group of mice using Picrosirius red staining for cross-referencing, so as to avoid possible overestimation of the effect of Masson's trichrome on myocardial fibrosis under acidic conditions (ISO-induced acute myocardial injury). The results of Picrosirius red staining and Masson's trichrome staining were found to be generally consistent. Notably, ISO mainly induced increases in type I and type III collagen, whereas inhibition of MEG3 blunted the ISO-induced increases in type I and type III collagen. This is consistent with the results of Wu et al. [26]. These findings support the hypothesis that inhibition of MEG3 can effectively

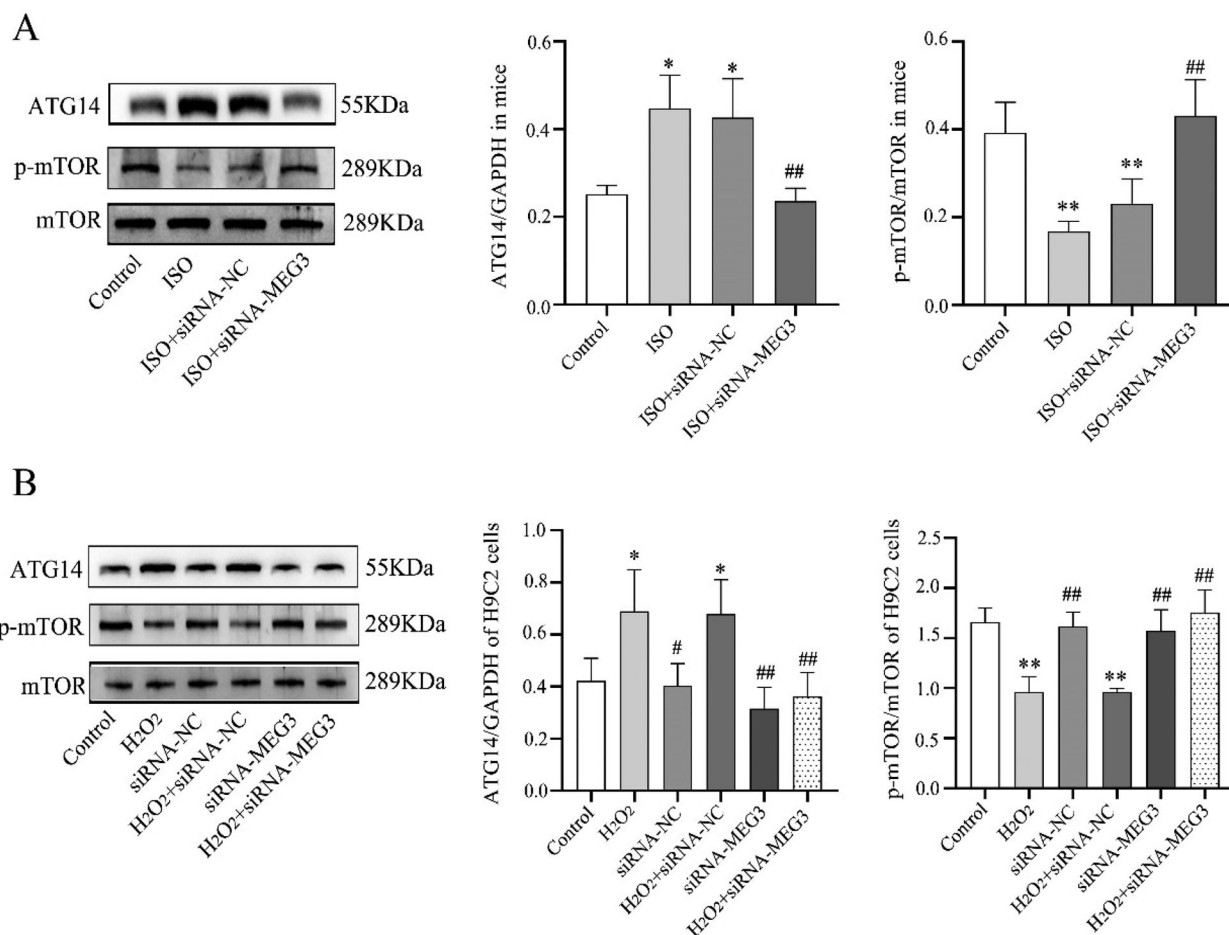


Figure 6. siRNA-MEG3 regulated the expression levels of ATG14 and p-mTORC1 protein. (A) Representative image of Western blotting of ATG14 and p-mTORC1 in mice and their quantitative analysis. (B) Representative image of Western blotting of ATG14 and p-mTORC1 in H9C2 cells and their quantitative analysis. Data are expressed as mean \pm SD. Mice, $n = 5$, H9C2 cells = 2 batches of cells, repeat 2~3 multiple wells for each batch of cells. * $p < 0.05$, ** $p < 0.01$ versus control group; # $p < 0.05$, ## $p < 0.01$ versus control group.

ameliorate cardiomyocyte hypertrophy and myocardial fibrosis [3,4].

In addition, our study found that the treatment of siRNA-MEG3 treatment significantly reduced ISO and H₂O₂ induced cardiomyocyte apoptosis. During the progression of HF, cardiomyocyte apoptosis is an important part of cardiac remodeling. It reduces myocardial contractility and causes cardiac dysfunction [27]. Apoptosis can be initiated by two main pathways: the extrinsic or death receptor pathway and the intrinsic or mitochondrial pathway. Although the activation of each pathway is distinct, they influence each other [28]. In particular, mitochondrially initiated events are regulated by a family of Bcl-2 proteins which reside in the outer mitochondrial membrane [29]. This family of proteins is composed of pro- (e.g. Bax, Bak, Bid, Puma) and anti-apoptotic (e.g. Bcl-2, Mcl-1) proteins. The Bcl-2 proteins play an important role in maintaining cardiomyocyte viability in response to stress [30]. The value of Bcl2/Bax is often used to evaluate the level of apoptosis, and a low value of Bcl2/Bax indicates a high level of apoptosis. In our study, inhibition of MEG3 ameliorates cardiomyocyte apoptosis are evidenced by significantly increasing the ratio of apoptosis molecular markers Bcl2/Bax in vivo and in vitro, and significantly reduces cardiomyocyte apoptosis under oxidative stress conditions. Some studies reported that inhibition of MEG3 could reduce cardiomyocyte apoptosis induced by hypoxia or high glucose, but they were mainly

in vitro studies without the support of animal experiments [31,32]. The above results suggest that siRNA-MEG3 has a protective effect on cardiomyocyte apoptosis under both in vivo and vitro oxidative stress conditions, and that this effect mainly involves the mitochondrial apoptosis pathway.

Oxidative stress is closely associated with the development of cardiac hypertrophy, and the transition from myocardial hypertrophy to heart failure leads to increased mitochondrial damage and oxidative stress [33], resulting in myocardial apoptosis and a significant decline in cardiac function. Previous studies have shown that ISO-treated ventricular tissue sections had significantly increased levels of H₂O₂ in Krebs-Hepes buffer [34]. DHE staining is mainly used as a fluorescent probe to detect ROS production with specificity for superoxide anion and hydrogen peroxide [35]. Therefore, we performed DHE staining after stimulation of cardiomyocytes with H₂O₂ and observed the effect of siRNA-MEG3 on H₂O₂-stimulated cardiomyocytes.

Our results demonstrated that inhibition of MEG3 significantly reduced the H₂O₂-induced increase in ROS levels in cardiomyocytes. Our results also showed that Tiron, a specific superoxide anion inhibitor, reduced ISO-induced ROS levels, while siRNA-MEG3 had the same effect. In addition, the combination of Tiron and siRNA-MEG3 reduced the ISO-induced increase in ROS levels more than Tiron alone, although there was no significant difference between the two. These results suggest, at least in part,

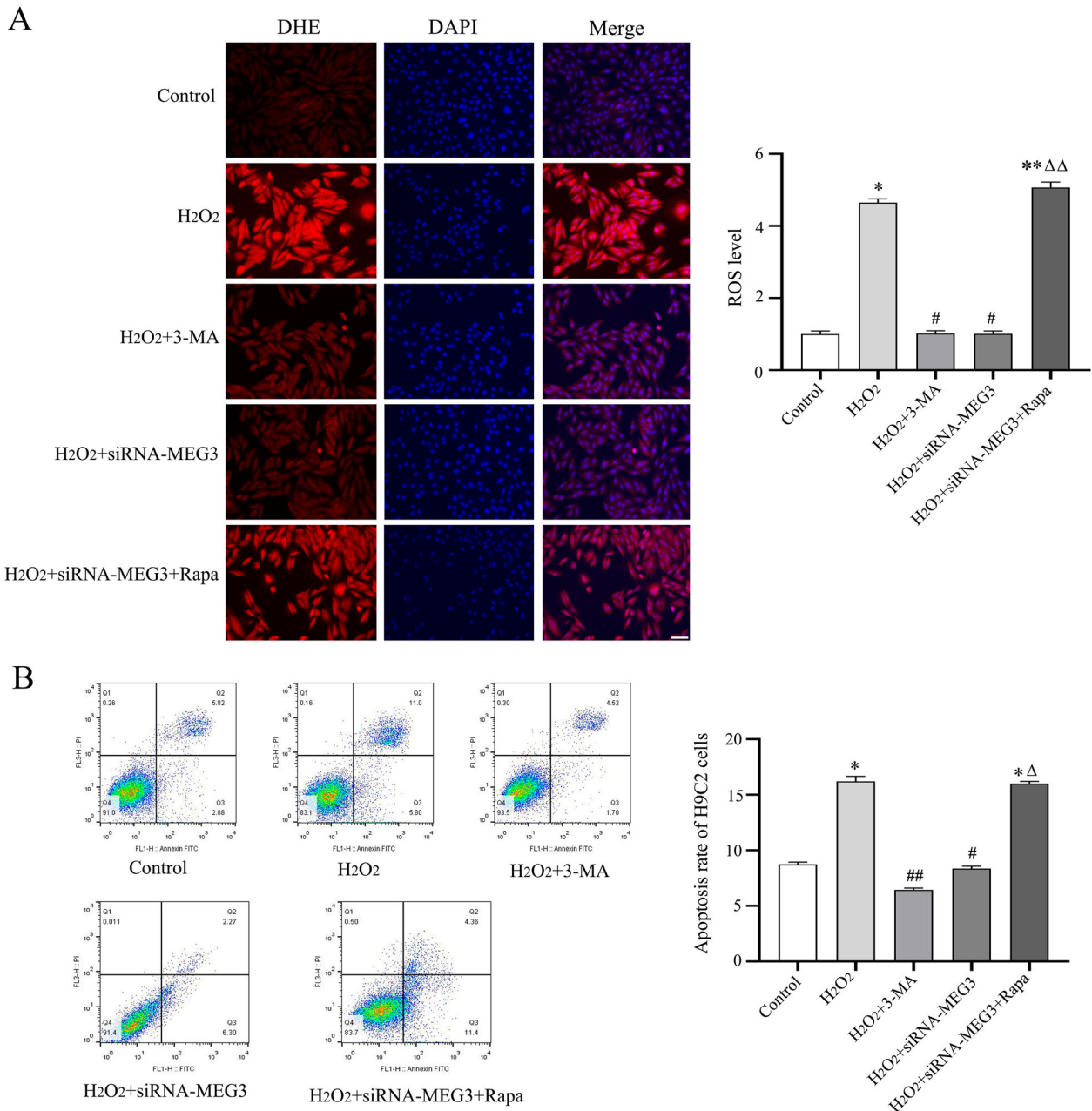


Figure 7. siRNA-MEG3 reduces H₂O₂-induced cardiomyocyte apoptosis and ROS levels by inhibiting autophagy. (A) Representative image of DHE immunofluorescence staining of H9C2 cells (scale bar = 50 μm) and quantitative analysis of DHE fluorescence density in H9C2 cells. Blue fluorescence represents the nucleus stained with DAPI, and red fluorescence represents ROS. (B) Representative images of flow cytometry in H9C2 cells and quantitative analysis of apoptotic cells. Data are expressed as mean ± SD, H9C2 cells = 2 batches of cells, repeat 2~3 multiple wells for each batch of cells. **p* < 0.05, ***p* < 0.01 versus control group; #*p* < 0.05, ##*p* < 0.01 versus H₂O₂ group; Δ*p* < 0.05, ΔΔ*p* < 0.01 H₂O₂ + siRNA-MEG3 + Rapa versus H₂O₂ + siRNA-MEG3.

that siRNA-MEG3 may inhibit ISO-induced excessive oxidative stress in cardiomyocytes by reducing superoxide anion or H₂O₂ levels.

A potential mechanism regarding the regulation of cardiomyocyte apoptosis by MEG3 under oxidative stress conditions may be through its direct target miR-129-5p.

It has been reported that MEG3 could target and inhibit the expression of miR-129-5p and silencing of MEG3 effectively promoted the therapeutic effect of dexmedetomidine on the neonatal mice with hypoxic-ischemic brain injury [5]. Our results showed that siRNA-MEG3 treatment reversed the decrease of miRNA-129-5p gene and p-Akt, p-GSK3β protein expression in murine LV of HF induced by ISO or H₂O₂-stimulated H9C2 cells. Studies have confirmed that ATG14 functions as miR-129-5p sponge and regulates the post-transcriptional activity of miR-129-5p and ultimately

regulates the expression of Bcl-2/Bax [6]. PI3 K/Akt is a pathway related to growth and proliferation, and activated Akt can activate or inhibit its downstream target protein GSK-3β through phosphorylation to play a regulatory role. GSK-3β is recognized as one of the substrates of PI3 K/Akt in the body, which can adjust the ratio of Bax, and then regulate cell cycle and apoptosis [36]. Recent data indicated that miR-1298 mimic reduced apoptosis in ischemia-reperfusion injured cardiomyocytes by increasing the protein expression of Bcl-2 and p-GSK3β and decreasing the protein expression of Bax [37]. Our results are similar to this. In conclusion, siRNA-MEG3 inhibits cardiomyocyte apoptosis by upregulating miR-129-5p and activating the Akt/GSK3β signaling pathway.

Autophagy is an intracellular catabolic process that degrades or recycles defective cellular components and

cytosolic protein aggregates. It plays a homeostatic role in cardiac development under physiological conditions, which is fundamental to cardiovascular physiology [38]. However, overactivation of autophagy can lead to autophagic cell death. Zhu et al. found that cardiac autophagy induced by chronic load was an inappropriate response that contributed to the progression of heart failure [39]. Moreover, excessive autophagy activation caused by severe stress can destroy most of the cytoplasm and organelles, especially mitochondria and endoplasmic reticulum, leading to complete loss of all cellular functions and abnormal cell morphology, apoptosis and necrosis [40]. Therefore, preventing excessive autophagy may be an important way to improve heart failure in the treatment of HF. Our results confirmed that either ISO or H₂O₂ can induce an abnormal increase in the autophagy of cardiomyocytes, which was mainly reflected in the increase of Beclin1, LC3II/LC3I protein expression and the decrease in p62 protein expression. However,

inhibition of MEG3 reversed the protein expressions that are associated with autophagic cell death. Beclin-1 is one of the earliest discovered mammalian autophagic effectors. It can initiate the nucleation step of autophagy by forming a protein complex with PtdIns(3)-kinase (Vps34) to initiate autophagic flux, and can also participate in the subsequent steps of autophagosome and lysosome fusion [41]. LC3II is converted from LC3I by ubiquitination and is a marker of autophagosome formation [42]. As an autophagy receptor, p62 can bind to LC3 and ubiquitinated substrates, which are then integrated into autophagosomes and can be degraded by autophagic lysosomes [43,44]. When autophagy is activated, autophagosomes fuse with lysosomes, and p62 proteins or organelles in autophagic vesicles are degraded by lysosomal enzymes, thereby decreasing p62 levels and increasing flux. Our results suggest that siRNA-MEG3 significantly inhibited the over-activation of autophagy induced by ISO and H₂O₂ and restored the autophagic flux.

To further investigate the mechanism of MEG3 inhibition in reducing ISO or H₂O₂-induced cardiac autophagy, we determined the expression levels of related autophagic proteins ATG14 and mTOR. The results showed that siRNA-MEG3 treatment reversed the ISO-induced increase in ATG14 expression and decreased expression of p-mTOR protein in the mouse model of HF. Both in vitro and in vivo experiments showed consistent results. ATG14 is a specific subunit of the PI3 K complex that targets the PI3 K complex to a possible site of autophagosome formation, thereby sorting the complex and enabling the PI3 K complex to play a specific role in autophagy. It has been reported [6] that miR-129-5p can inhibit H₂O₂-induced autophagy and apoptosis in H9c2 cells by downregulating ATG14 and activating the PI3 K/AKT/mTOR pathway. The PI3 K/Akt/mTOR signaling pathway is a typical autophagy signaling pathway [45] that negatively regulates autophagy. As a serine/threonine kinase, mTOR is a key upstream target molecule for the negative regulation of autophagy [46].

There are two different complexes of mTORC1 and mTORC2 in the cell. The mTORC2 mainly regulates cell survival and cytoskeleton, and can activate mTORC1 by phosphorylating Akt. mTORC1 is mainly related to promoting cell growth and metabolism. It can inhibit autophagy by binding to ULK1 (unc-51-like kinase 1) complex. Furthermore, our results showed that the mTORC1 blocker rapamycin abolished the inhibitory effect of siRNA-MEG3 on H₂O₂-induced

cell apoptosis and ROS production. The autophagy inhibitor 3-MA, similar to siRNA-MEG3, reduced H₂O₂-induced apoptosis and ROS levels in cardiomyocytes. These results suggest that siRNA-MEG3 may inhibit ISO and H₂O₂ induced cardiomyocyte autophagy by regulating the miRNA-129/ ATG14/ AKT/ mTORC1 signaling pathway, and that siRNA-MEG3 alleviates cardiomyocyte apoptosis during excessive oxidative stress by inhibiting autophagy.

In conclusion, this study highlights the novel aspects of MEG3-mediated cardiac remodeling and dysfunction in response to ISO-induced HF and disease progression.

We demonstrated for the first time that siRNA-MEG3 significantly reduced cardiomyocyte autophagy and apoptosis induced by ISO or H₂O₂, possibly through the miRNA-129/ ATG14/AKT signaling pathway, and that siRNA-MEG3 down-regulated cardiomyocyte apoptosis, possibly by inhibiting autophagy. The results of this study indicate that inhibition of MEG3 may have a therapeutic potential in the treatment of maladaptive cardiac remodeling and HF.

Acknowledgments

This study was supported by science and technology key projects of Henan Province, China (No. 212102310586 to Heqin Zhan).

Data availability statement

The authors confirm that the data supporting the findings of this study are available within the article [and/or] its supplementary materials.

Disclosure statement

No potential conflict of interest was reported by the author(s).

Funding

This work was supported by Science and technology key projects of Henan Province, China: [Grant Number 212102310586].

References

- [1] Batkai S, Genschel C, Viereck J, et al. CDR132L improves systolic and diastolic function in a large animal model of chronic heart failure. *Eur Heart J*. 2021;42(2):192–201. doi:10.1093/eurheartj/ehaa791
- [2] Gao G, Chen W, Yan M, et al. Rapamycin regulates the balance between cardiomyocyte apoptosis and autophagy in chronic heart failure by inhibiting mTOR signaling. *Int J Mol Med*. 2020;45(1):195–209.
- [3] Piccoli MT, Gupta SK, Viereck J, et al. Inhibition of the Cardiac Fibroblast-Enriched lncRNA Meg3 Prevents Cardiac Fibrosis and Diastolic Dysfunction. *Circ Res*. 2017;121(5):575–583. doi:10.1161/CIRCRESAHA.117.310624
- [4] Zhang J, Liang Y, Huang X, et al. STAT3-induced upregulation of lncRNA MEG3 regulates the growth of cardiac hypertrophy through miR-361-5p/HDAC9 axis. *Sci Rep*. 2019;9(1):460. doi:10.1038/s41598-018-36369-1
- [5] Zhou XM, Liu J, Wang Y, et al. Silencing of long noncoding RNA MEG3 enhances cerebral protection of dexmedetomidine against hypoxic-ischemic brain damage in neonatal mice by binding to miR-129-5p. *J Cell Biochem*. 2018.
- [6] Zhang H, Zhang X, Zhang J. MiR-129-5p inhibits autophagy and apoptosis of H9c2 cells induced by hydrogen peroxide via the PI3 K/AKT/mTOR signaling pathway by targeting ATG14. *Biochem Biophys Res Commun*. 2018;506(1):272–277. doi:10.1016/j.bbrc.2018.10.085
- [7] Zhang N, Zhang Y, Qian H, et al. Selective targeting of ubiquitination and degradation of PARP1 by E3 ubiquitin ligase WWP2

- regulates isoproterenol-induced cardiac remodeling. *Cell Death Differ.* 2020;27(9):2605–2619. doi:10.1038/s41418-020-0523-2
- [8] Jin W, Zhang Y, Xue Y, et al. Crocin attenuates isoprenaline-induced myocardial fibrosis by targeting TLR4/NF-kappaB signaling: connecting oxidative stress, inflammation, and apoptosis. *Naunyn Schmiedeberg Arch Pharmacol.* 2020;393(1):13–23. doi:10.1007/s00210-019-01704-4
- [9] Ghorbanzadeh V, Jafarpour A, Pirnia A, et al. The role of vasopressin V1A and oxytocin OTR receptors in protective effects of arginine vasopressin against H2O2-induced oxidative stress in H9C2 cells. *Arch Physiol Biochem.* 2022;128(3):830–835. doi:10.1080/13813455.2020.1729816
- [10] Lee JH, Kim DH, Kim M, et al. Mitochondrial ROS-mediated metabolic and cytotoxic effects of isoproterenol on cardiomyocytes are p53-dependent and reversed by curcumin. *Molecules.* 2022;27(4):1346. doi:10.3390/molecules27041346
- [11] Modesti A, Bertolozzi I, Gamberi T, et al. Hyperglycemia activates JAK2 signaling pathway in human failing myocytes via angiotensin II-mediated oxidative stress. *Diabetes.* 2005;54(2):394–401. doi:10.2337/diabetes.54.2.394
- [12] Liu X, Tong Z, Chen K, et al. The role of miRNA-132 against apoptosis and oxidative stress in heart failure. *Biomed Res Int.* 2018;2018:3452748.
- [13] Su M, Wang J, Wang C, et al. MicroRNA-221 inhibits autophagy and promotes heart failure by modulating the p27/CDK2/mTOR axis. *Cell Death Differ.* 2015;22(6):986–999. doi:10.1038/cdd.2014.200
- [14] Gustafsson AB, Gottlieb RA. Recycle or die: the role of autophagy in cardioprotection. *J Mol Cell Cardiol.* 2008;44(4):654–661. doi:10.1016/j.yjmcc.2008.01.010
- [15] Wang L, Gao M, Chen J, et al. Resveratrol ameliorates pressure overload-induced cardiac dysfunction and attenuates autophagy in rats. *J Cardiovasc Pharmacol.* 2015;66(4):376–382. doi:10.1097/FJC.0000000000000290
- [16] Hang P, Zhao J, Su Z, et al. Choline inhibits ischemia-reperfusion-induced cardiomyocyte autophagy in Rat myocardium by activating Akt/mTOR signaling. *Cell Physiol Biochem.* 2018;45(5):2136–2144. doi:10.1159/000488049
- [17] Senoner T, Dichtl W. Oxidative Stress in Cardiovascular Diseases: still a therapeutic target? *Nutrients.* 2019;11(9).
- [18] Zhan H, Huang F, Niu Q, et al. Downregulation of miR-128 ameliorates Ang II-induced cardiac remodeling via SIRT1/PIK3R1 multiple targets. *Oxid Med Cell Longev.* 2021;2021:8889195.
- [19] van der Pol A, van Gilst WH, Voors AA, et al. Treating oxidative stress in heart failure: past, present and future. *Eur J Heart Fail.* 2019;21(4):425–435. doi:10.1002/ejhf.1320
- [20] Fan C, Tang X, Ye M, et al. Qi-Li-Qiang-Xin alleviates isoproterenol-induced myocardial injury by inhibiting excessive autophagy via activating AKT/mTOR pathway. *Front Pharmacol.* 2019;10:1329. doi:10.3389/fphar.2019.01329
- [21] Attalla DM, Ahmed LA, Zaki HF, et al. Paradoxical effects of atorvastatin in isoproterenol-induced cardiotoxicity in rats: role of oxidative stress and inflammation. *Biomed Pharmacother.* 2018;104:542–549. doi:10.1016/j.biopha.2018.05.005
- [22] Park WH. MAPK inhibitors, particularly the JNK inhibitor, increase cell death effects in H2O2-treated lung cancer cells via increased superoxide anion and glutathione depletion. *Oncol Rep.* 2018;39(2):860–870.
- [23] Tsutsui H, Kinugawa S, Matsushima S. Oxidative stress and heart failure. *Am J Physiol Heart Circ Physiol.* 2011;301(6):H2181–H2190. doi:10.1152/ajpheart.00554.2011
- [24] Sun Y, Xie Y, Du L, et al. Inhibition of BRD4 attenuates cardiomyocyte apoptosis via NF-kappaB pathway in a rat model of myocardial infarction. *Cardiovasc Ther.* 2018;36(2).
- [25] Chen J, Huang ZP, Seok HY, et al. mir-17-92 cluster is required for and sufficient to induce cardiomyocyte proliferation in postnatal and adult hearts. *Circ Res.* 2013;112(12):1557–1566. doi:10.1161/CIRCRESAHA.112.300658
- [26] Wu X, Li M, Chen SQ, et al. Pin1 facilitates isoproterenol-induced cardiac fibrosis and collagen deposition by promoting oxidative stress and activating the MEK1/2-ERK1/2 signal transduction pathway in rats. *Int J Mol Med.* 2018;41(3):1573–1583.
- [27] Yan X, Wu H, Ren J, et al. Shenfu Formula reduces cardiomyocyte apoptosis in heart failure rats by regulating microRNAs. *J Ethnopharmacol.* 2018;227:105–112. doi:10.1016/j.jep.2018.05.006
- [28] D'Arcy MS. Cell death: a review of the major forms of apoptosis, necrosis and autophagy. *Cell Biol Int.* 2019;43(6):582–592. doi:10.1002/cbin.11137
- [29] Cory S, Adams JM. The Bcl2 family: regulators of the cellular life-or-death switch. *Nat Rev Cancer.* 2002;2(9):647–656. doi:10.1038/nrc883
- [30] Virzi GM, Clementi A, Ronco C. Cellular apoptosis in the cardiorenal axis. *Heart Fail Rev.* 2016;21(2):177–189. doi:10.1007/s10741-016-9534-y
- [31] Zhao LY, Li X, Gao L, et al. LncRNA MEG3 accelerates apoptosis of hypoxic myocardial cells via FoxO1 signaling pathway. *Eur Rev Med Pharmacol Sci.* 2019 Aug;23(3 Suppl):334–340.
- [32] Chen Y, Zhang Z, Zhu D, et al. Long non-coding RNA MEG3 serves as a ceRNA for microRNA-145 to induce apoptosis of AC16 cardiomyocytes under high glucose condition. *Biosci Rep.* 2019 Jun 28;39(6).
- [33] Osterholt M, Nguyen TD, Schwarzer M, et al. Alterations in mitochondrial function in cardiac hypertrophy and heart failure. *Heart Fail Rev.* 2013;18(5):645–656. doi:10.1007/s10741-012-9346-7
- [34] Lucas AMB, de Lacerda Alexandre JV, Araújo MTS, et al. Diazoxide modulates cardiac hypertrophy by targeting H2O2 generation and mitochondrial superoxide dismutase activity. *Curr Mol Pharmacol.* 2020;13(1):76–83. doi:10.2174/1874467212666190723144006
- [35] Ahmad A, Prakash R, Khan MS, et al. Enhanced antioxidant effects of naringenin nanoparticles synthesized using the high-energy ball milling method. *ACS Omega.* 2022;7(38):34476–34484. doi:10.1021/acsomega.2c04148
- [36] Zhang H, Dong R, Zhang P, et al. Songorine suppresses cell growth and metastasis in epithelial ovarian cancer via the Bcl2/Bax and GSK3beta/betacatenin signaling pathways. *Oncol Rep.* 2019;41(5):3069–3079.
- [37] Ouyang C, Huang L, Ye X, et al. Overexpression of miR-1298 attenuates myocardial ischemia-reperfusion injury by targeting PP2A. *J Thromb Thrombolysis.* 2022;53(1):136–148. doi:10.1007/s11239-021-02540-1
- [38] Nandi SS, Katsurada K, Sharma NM, et al. MMP9 inhibition increases autophagic flux in chronic heart failure. *Am J Physiol Heart Circ Physiol.* 2020;319(6):H1414–H1437. doi:10.1152/ajpheart.00032.2020
- [39] Zhu H, Tannous P, Johnstone JL, et al. Cardiac autophagy is a maladaptive response to hemodynamic stress. *J Clin Invest.* 2007;117(7):1782–1793. doi:10.1172/JCI27523
- [40] Nishida K, Yamaguchi O, Otsu K. Crosstalk between autophagy and apoptosis in heart disease. *Circ Res.* 2008;103(4):343–351. doi:10.1161/CIRCRESAHA.108.175448
- [41] Sun Y, Yao X, Zhang QJ, et al. Beclin-1-Dependent autophagy protects the heart during sepsis. *Circulation.* 2018;138(20):2247–2262. doi:10.1161/CIRCULATIONAHA.117.032821
- [42] Ren PH, Zhang ZM, Wang P, et al. Yangxinkang tablet protects against cardiac dysfunction and remodeling after myocardial infarction in rats through inhibition of AMPK/mTOR-mediated autophagy. *Pharm Biol.* 2020;58(1):321–327. doi:10.1080/13880209.2020.1748662
- [43] He R, Peng J, Yuan P, et al. Divergent roles of BECN1 in LC3 lipidation and autophagosomal function. *Autophagy.* 2015;11(5):740–747. doi:10.1080/15548627.2015.1034404
- [44] Lin X, Li S, Zhao Y, et al. Interaction domains of p62: a bridge between p62 and selective autophagy. *DNA Cell Biol.* 2013;32(5):220–227. doi:10.1089/dna.2012.1915
- [45] Zhang X, Yang K, Zhang H, et al. Effect of typhaneoside on ventricular remodeling and regulation of PI3 K/Akt/mTOR pathway. *Herz.* 2020 Dec;45(Suppl 1):113–122.
- [46] Chen X, Li M, Chen D, et al. Autophagy induced by calcium phosphate precipitates involves endoplasmic reticulum membranes in autophagosome biogenesis. *PLoS One.* 2012;7(12):e52347. doi:10.1371/journal.pone.0052347